Heteropolytungstate-decorated core-shell magnetic nanoparticles: A covalent strategy for polyoxometalate-based hybrid nanomaterials

Ourania Makrygenni, Emilie Secret, Aude Michel, Dalil Brouri, Vincent Dupuis, Anna Proust, Jean-Michel Siaugue, Richard Villanneau

Heteropolytungstate-decorated core-shell magnetic nanoparticles: a covalent strategy for Polyoxometalate-based hybrid nanomaterials

Ourania Makrygenni,[a] *Emilie Secret,*[b] *Aude Michel,*[b] *Dalil Brouri,*[c] *Vincent Dupuis,*[b] *Anna Proust,*[a] *Jean-Michel Siaugue,**[b] *Richard Villanneau**[a]

[a] Sorbonne Universités, UPMC-Paris 06, CNRS UMR 8232, Institut Parisien de Chimie Moléculaire, 4 Place Jussieu, F-75005 Paris, France.
[b] Sorbonne Universités, UPMC-Paris 06, CNRS UMR 8234, Physicochimie des Électrolytes et Nanosystèmes Interfaciaux, 4 Place Jussieu, F-75005 Paris, France
[c] Sorbonne Universités, UPMC-Paris 06, CNRS UMR 7197, Laboratoire de Réactivité de Surface, 4 Place Jussieu, F-75005 Paris, France.

Corresponding Authors
* at Sorbonne Universités, UPMC-Paris 06, CNRS UMR 8232, Institut Parisien de Chimie Moléculaire, 4 Place Jussieu, F-75005 Paris, France. E-mail: richard.villanneau@upmc.fr
*at Sorbonne Universités, UPMC-Paris 06, CNRS UMR 8234, Physicochimie des Électrolytes et Nanosystèmes Interfaciaux, 4 Place Jussieu, F-75005 Paris, France. E-mail: jean-michel.siaugue@upmc.fr

Graphical Abstract

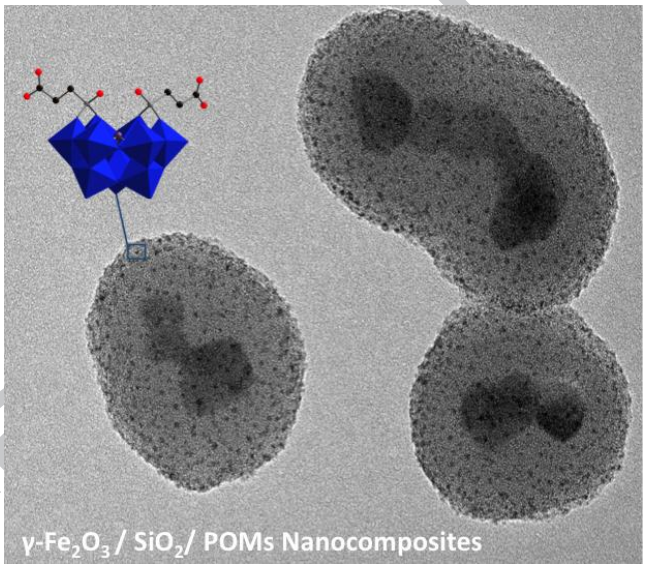

Keywords

Core-shell nanoparticles; polyoxometalates; hybrid materials; HR-TEM.

Abstract

Amino-functionalized core-shell magnetic nanoparticles have been covalently grafted with Polyoxometalates (POMs). These multifunctional nanocomposites have been obtained through the coupling of heteropolytungstate-based hybrids bearing carboxylic acid functions with aminopropyl functions that decorate the core-shell nanoparticles. The physical properties of the resulting materials have been studied by a large set of techniques. The very good nanostructuration of the POMs at the surface of the obtained nanoparticles have thus been directly observed by high-resolution transmission electronic microscopy (HR-TEM). Furthermore, the hyperthermia properties of these nanocomposites have been also considered as a function of the size of the magnetic core. Finally, the stability of these suspensions in

organic media makes them particularly interesting in the frame of their processing or their potential use as nanocatalysts.

1. Introduction

The immobilization of homogeneous catalysts onto heterogeneous support has now been being studied for decades and various strategies were developed as a function of the targeted reactions/catalysts/supports. In all cases, particular attention was paid to the leaching properties (*i.e*. the strength of the link between both partners) and the recyclability of the catalyst at once. In the case of polyoxometalate catalysts (nanosized early-transition metal oxoclusters = POMs), several efficient strategies were described [1]. POMs may thus be successfully and strongly immobilized into materials through their encapsulation into metal-organic frameworks (MOF) [2,3], their intercalation into layered double hydroxides [4], their one-pot embedding into a silica matrix *via* co-condensation sol-gel methods [5] or the covalent grafting of vacant POMs into the walls of hybrid supports [6,7,8].

In this respect, R. Villanneau and co-workers recently focused on the use of vacant organophosphonyle/arsonyle derivatives of heteropolytungstates, bearing reactive pending organic functions. These were then reacted with complementary functions grafted onto the walls of organically modified mesoporous silicas. This so-called "post-functionalization" strategy is currently used for the elaboration of POMs-based materials [9]. The use of very efficient coupling agents led to the preparation of well-ordered materials, with a regular distribution of isolated POMs at the periphery of the micropores. This remarkable nanostructuration was directly evidenced through the use of high-resolution transmission electronic microscopy, due to the high electronic density of tungsten atoms of the POMs [10]. One important conclusion of this work was the correlation observed between the catalytic efficiency and the structuration of the active species at the surface of the support, despite the decrease of the textural properties of this support after each functionalization step.

Furthermore, silica nanoparticles used as a catalytic support may have a higher catalyst loading capacity and a higher specific surface than many extended support matrices. Such materials would certainly lead to an improved catalytic activity but conventional separation methods may become inefficient for particle sizes below 100 nm. The incorporation of magnetic cores such as iron oxides into the silica shell offers then an elegant solution to this limitation, through their magnetic separation. Astonishingly, the use of such core-shell magnetic nanoparticles (MNPs) for the immobilization of catalysts is poorly described in the literature [11] (especially for POMs catalysts), despite their potential for magnetic separation. However considerable efforts were spent for controlling the synthesis, the stability, the magnetic properties but also the structure of the coating surfaces of this particular class of nano-objects [12]. Actually, the control over the synthesis conditions and the surface functionalization allowed their use in different fields. It led indeed to the understanding of their biological behaviour for applications in pharmaceutical and biomedical areas but also of their superparamagnetic properties for applications in materials science [13]. Magnetic nanoparticles are also currently attracting attention because of additional intrinsic properties, that is their high electronic density and their hyperthermic behaviour in the presence of oscillating magnetic fields. Both properties recently led to their use respectively as contrast agents for magnetic resonance imaging (MRI) and heating mediators for cancer thermotherapy [14].

In a recent work, the group of J. M. Siaugue thus prepared core-shell MNPs composed of a core of superparamagnetic maghemite nanoparticles embedded in a silica matrix enriched with rhodamine molecules for fluorescence imaging [15]. Moreover, their surface was functionalized with short PEG chains in order to ensure their stabilization. These

nanocomposites were then used for the spatiotemporal regulation of protein distribution in the cytoplasm of a HeLa cell [16].

In the present manuscript, we report on the synthesis and characterization of new hybrids materials obtained by the covalent grafting of POM-based hybrids onto the surface of functionalized core-shell MNPs. As a result, several issues were addressed in this work: (i) the optimization of the isolation procedures for large size sorted maghemite nanoparticles and their encapsulation into silica shells, (ii) the stabilization of POMs-decorated MNPs suspensions in organic solvents (in view of their further use in catalytic oxidation processes, but also of their processing), (iii) the development of grafting methodology for both partners (POMs and MNPs), (iv) the characterization of grafted POMs at the nanoparticles surface and (v) the study of hyperthermia properties of the resulting hybrid nanomaterials.

2. Materials and methods

2.1. Materials and reagents.

Solvents and other reagents were obtained from commercial sources and used as received, except for triethylamine and acetonitrile, which were distilled over CaH_2. The complex $(^{n}Bu_4N)_3NaH[As^{III}W_9O_{33}\{P(O)(CH_2CH_2CO_2H)\}_2]$ - $TBA_3NaH(POM\text{-}CO_2H)$ was prepared as previously described (figure 1) [17].

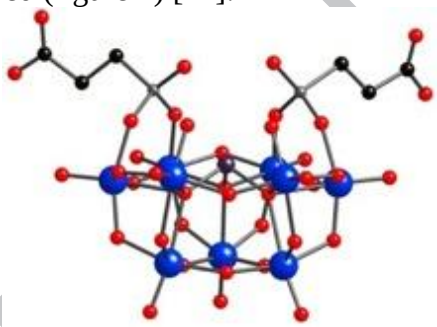

Fig. 1: Structural representation of the bis-propanoic acid phosphonyle derivative $[As^{III}W_9O_{33}\{P(O)(CH_2CH_2CO_2H)\}_2]^{5-}$ anion. The W, As, P, O and C atoms are shown respectively in blue, prune, grey, red and black.

2.2. Methods

The purity of $TBA_3NaH(POM\text{-}CO_2H)$ was verified by IR (recorded from KBr pellets on a Jasco FT/IR-4100) and ^{1}H and ^{31}P NMR solution spectroscopy (recorded in 5 mm o.d. tubes on a Bruker Avance II 300 spectrometer equipped with a QNP probehead). X-Ray Fluorescence analyses were conducted with an energy dispersive spectrometer XEPOS with Turboquant powder software. Atomic absorption (flame spectroscopy) measurements for iron analysis were performed with a Perkin-Elmer Analyst 100 spectrophotometer. HR-TEM analyses were realized on a microscope operating at 200 kV with a resolution of 0.18 nm (JEOL JEM 2011 UHR) equipped with an XEDS system (PGT IMIX-PC). Samples were deposited on Cu grid covered with an amorphous carbon film.

X-ray photoelectron spectroscopy (XPS) spectra were performed on an Omicron (ESCA+) spectrometer, using an Al Kα X-ray source (1486.6 eV) equipped with a flood gun. Magnetic measurements were performed on an MPMS-XL7 Superconducting Quantum Interference Device. Magnetic hyperthermia properties of the nanoparticles were measured by recording the temperature of the nanoparticles solution with a nonmetallic optical fiber thermometer (Fluoroptic, Luxtron) while excited by a magnetizing coil of a commercial radiofrequency ac magnetic field generator (MagneTherm, NanoTherics). A frequency of 535 Hz and a field of 21.4 mT were used in this experiment. Dynamic Light Scattering measurements were performed on a Malvern Zetasizer Nano S system.

2.3. Synthetic procedures

2.3.1 Synthesis of unsorted maghemite nanoparticles

The unsorted maghemite nanoparticles were synthesized following a modified version of the usual Massart's co-precipitation method [18]. First, 1 L of a 22.5 % ammonia solution was quickly added to an acidic solution iron (II) and iron (III) ions (180 g of $FeCl_2$, 100 mL of HCl 37%, 500 mL of deionized water, 715 mL of $FeCl_3$ 27%, completed to 3 L with deionized water). After 30 min of stirring, the obtained Fe_3O_4 nanoparticles were washed with deionized water, and redispersed in 360 mL of nitric acid (52 %). Then a solution of iron(III) nitrate (323 g in 800 mL of deionized water) was added to the nanoparticles and the solution was boiled and agitated for 30 min, in order to oxidize the Fe_3O_4 nanoparticles into γ-Fe_2O_3 nanoparticles. The resulting nanoparticles were then washed with nitric acid once (52 %, 360 mL), with acetone 3 times, and with diethylether twice. They were finally redispersed in deionized water. In order to be stable at neutral pH, the nanoparticles were finally citrated by heating the nanoparticles with sodium citrate for 30 min. The quantity of sodium citrate introduced at this step was fixed as to obtain an n_{Cit}/n_{Fe} ratio of 0.13. After being rinsed with acetone and diethylether, the resulting nanoparticles were dispersed in deionized water (maghemite solution **1**). The final iron concentration was found equal to 1 $mol.L^{-1}$ as measured by flame spectroscopy.

2.3.2 Synthesis of sorted maghemite nanoparticles

The sorted maghemite nanoparticles were obtained by an inverse Massart's co-precipitation method. Indeed, the acidic equimolar iron (II) and iron (III) ions solution (124.25 g of $FeCl_2$, 50 mL of HCl 37%, 250 mL of deionized water, 293.5 mL of $FeCl_3$ 27%) was added dropwise over 4 h to 2 L of 5 % ammonia in water, under agitation. The washing and oxidation steps were then the same as above. After redispersion, the γ-Fe_2O_3 nanoparticles were polydispersed in size. In order to decrease the polydispersity, 10 mL of nitric acid (52.5 %) were added to the solution. The addition of nitric acid increases the ionic strength leading to flocculation of the larger, thus less stable, nanoparticles. These precipitated nanoparticles were separated from the rest of the ferrofluid, rinsed with acetone and diethyl ether, and finally redispersed in deionized water. In order to ensure their stability and dispersion at neutral pH, the nanoparticles were finally citrated by heating with sodium citrate for 30 min. After being rinsed with acetone and diethylether, the resulting nanoparticles were dispersed in deionized water (maghemite solution **2**). The final iron concentration was found equal to 0.86 $mol.L^{-1}$.

2.3.3 Synthesis of amino-functionalized core-shell MNPs with unsorted cores

In a bottle of 250 mL we introduced 400 µL of maghemite solution **1** (c_{Fe}=1 $mol.L^{-1}$, n_{Fe}=0.4 mmol). Afterwards, 25 mL of distilled water and 50 ml of absolute ethanol were inserted to the solution. The mixture was agitated for a couple of minutes before introducing 600 µL of tetraethoxyorthosilicate (TEOS, n=2.69 mmol) and 1.25 mL of a 30% ammonia solution (n=5.975 mmol). The resulting dispersion was stirred for 2 additional hours. The functionalization of the silica shell by PEG chains and $-NH_2$ functions was carried out by the addition of 200 µL of TEOS (n=0.897 mmol), 230 µL of 3-[methoxy(polyethyleneoxy)propyl]trimethoxysilane (PEOS, (n=0.424 mmol) and finally 100 µL of aminopropyltriethoxysilane (APTES, n=0.427 mmol). The mixture was stirred overnight. The washing procedure was carried out by 3 successive centrifugations of the solution at 10.000 rpm with absolute ethanol. Each washing step was followed by

ultrasonication to completely disperse the NPs. These NPs were finally dispersed in 25 mL of freshly distilled acetonitrile, followed by several minutes of sonication.

2.3.4 Synthesis of amino-functionalized core-shell MNPs with sorted cores

The synthesis of core-shell NPs with sorted cores followed the same principle as the one mentioned above for the core-shell NPs with unsorted cores. The synthesis was performed in two steps: the condensation of TEOS was followed by the functionalization of the silica shell by PEG chains and amino groups. For the 1st step, 1.20 mL of maghemite solution **2** (c_{Fe}=0.86 mol.L^{-1}, n_{Fe}=1.03 mmol) with 25 mL of distilled water and 50 mL of absolute ethanol were added into a 100 mL flask. Then, 1.30 mL of TEOS (n=5.87 mmol) and 1.25 mL of 30% ammonia solution (n=5.975 mmol) were inserted to the mixture and the later was stirred for 2 hours. The second step consisted in the addition of 450 µL of TEOS (n=2.02 mmol), 495 µL of PEOS (n=0.91 mmol) and 225 µL of APTES (n=0.96 mmol). The mixture was agitated for 24 hours. The washing approach was the same as stated before for the unsorted NPs. Finally, the NPs were dispersed in 25 mL of freshly distilled acetonitrile. At least 10 min of sonication were necessary to fully disperse the NPs in the organic medium.

2.3.5 Covalent grafting of $TBA_3NaH(POM\text{-}CO_2H)$ with the $\{NH_2\}$-functionalized core-shell MNPs

The synthetic procedure for the covalent grafting of $TBA_3NaH(POM\text{-}CO_2H)$ onto the $\{NH_2\}$-functionalized MNPs (with sorted or unsorted cores) was adapted from the protocol used for the covalent immobilization of POMs onto the surface of SBA-15 functionalized with aminopropyl groups [8]. Typically, 0.27 g (0.088 mmol/1 eq) of $TBA_3NaH(POM\text{-}CO_2H)$ were introduced in a 50 mL Schlenk tube and kept under vacuum for an overnight drying. The $TBA_3NaH(POM\text{-}CO_2H)$ complex was then dissolved in 2 mL of freshly distilled acetonitrile under nitrogen. Then 72.5 µL (0.525 mmol/6 eq) of triethylamine were added and the resulting mixture was cooled in an ice bath at -30 °C. After 30 min, isobutylchloroformiate (64.3 µL, 0.525 mmol/6 eq) was introduced and the solution was stirred for 30 min. In parallel, 25 mL of amino-functionalized core-shell MNPs dispersed in distilled acetonitrile were introduced in another Schlenk tube under nitrogen and were transferred to the latter solution *via* a cannula. The resulting dispersion was stirred overnight at room temperature in an inert atmosphere. The NPs were finally washed with acetonitrile 3 times by centrifugation (10000 rpm for 20 minutes).

2.3.6 Electrostatic deposition of $TBA_3NaH(POM\text{-}CO_2H)$ onto $\{NH_2\}$-functionalized core-shell MNPs

$TBA_3NaH(POM\text{-}CO_2H)$ (0.27 g, 0.088 mmol) was introduced in a 50 mL round-bottom flask containing 25 mL of amino-functionalized MNPs (with unsorted cores) dispersed in acetonitrile. The mixture was stirred for several days to have the highest initial tungsten amount possible. The NPs were washed with acetonitrile 3 times by centrifugation (10000 rpm for 20 minutes), and finally dispersed in acetonitrile. The final concentrations are identical before and after grafting the POMs since all the magnetic materials were easily recovered after each centrifugation or magnetic separation step from the organic solvent. The typical concentration of POMs-decorated magnetic nanoparticles are then in the range $5.5.10^{-7}$ - 10^{-6} mol.L^{-1} after redispersion, as checked by ICP measurements.

3. Results and discussion

Some recent examples of the association of POMs and MNPs can be found in the literature [19-22]. In most cases, these works correspond to simple deposition of HPAs (such as $H_3PM_{12}O_{40}$, M = W, Mo) onto the surface of silica-coated MNPs, or more rarely of amino-functionalized silica-coated MNPs [19]. These systems are generally used as nanocatalysts for catalytic acid–based processes, such as the formation of 5-ethoxymethylfurfural from glucose [20], or Mannich-type reactions [21], but examples in oxidation processes can also be found [22].

In order to avoid lixiviation effects, we aimed in this work at associating polyoxometalate-based hybrids with magnetic nanoparticles through stable covalent links, in view of using the resulting materials as magnetically separable nanocatalysts. For this purpose, we used organically modified magnetic core-shell nanoparticles and POM-based hybrids that contain complementary organic functions: an amine group for the MNPs and a carboxylic acid group for the POMs, leading to the formation of an amide function.

3.1 Preparation of magnetic core-shell nanoparticles

According to the procedures described in the group of Siaugue and coworkers, unsorted maghemite nanoparticles may be easily obtained in high concentration and large volume ($[Fe]_{final}$ *ca.* 1 $mol.L^{-1}$), with a low average size but also with a relatively high polydispersity. The maghemite nanoparticles obtained here had an average diameter of 7 nm. It is noteworthy that hyperthermia properties of the resulting materials were also addressed in the frame of this work. However, small polydisperse magnetic nanoparticles demonstrate poor hyperthermia properties [23]. In a second time, we thus prepared sorted maghemite NPs with an increased size (average diameter of 9 nm) and a less polydisperse size distribution, in order to obtain particles with better magnetic hyperthermia properties. The synthesis of this second batch of maghemite nanoparticles was performed through an inverse co-precipitation method, *i.e.* by a slow addition of the iron salts solution to the ammonia solution. This method led to the formation of larger nanoparticles. Then, as to decrease the polydispersity of the nanoparticles, a size sorting procedure was used, by destabilizing the larger particles with a small amount of nitric acid, and finally keeping the particles that flocculated [24].

The core-shell NPs (with sorted or unsorted maghemite cores) were obtained after embedding magnetic maghemite nanoparticles within a silica shell and functionalizing them with short polyethyleneglycol (PEG) chains and aminopropyl functions. Their synthesis and functionalization were performed through a two-step procedure: [25]

i) The first silica shell was prepared via the hydrolysis of TEOS serving as the sol-gel precursor. The condensation of TEOS onto citrated maghemite nanoparticles was achieved in ethanolic medium in the presence of ammonia.

ii) In a second step we carried out the silica shell functionalization with PEG chains and amino groups. Herein, a simultaneous condensation of amino silane and PEG silane derivative compounds, APTES and PEOS respectively, with the addition of a small amount of TEOS was accomplished.

Finally, titration of the $–NH_2$ functions (introduced after reaction with APTES) at the surface of the NPs was performed according to a classical titration technique (see ESI). In typical samples with unsorted or sorted cores, the $\{-NH_2\}$ concentration measured was $3.5.10^{-3}$ $mol.L^{-1}$ and $6.0.10^{-3}$ $mol.L^{-1}$ respectively. These values correspond to ca. 6500 $\{-NH_2\}$ functions per NP, *i.e* 1 $\{-NH_2\}$ function / nm^2 for unsorted cores, and ca. 6000 $\{-NH_2\}$ functions per NP, *i.e* 0.6 $\{-NH_2\}$ function / nm^2 for the sorted cores. This test was performed in conditions where the {-NH2} functions were not protonated.

3.2 Synthesis of POM-CO_2H-decorated core-shell MNPs.

The covalent grafting of POM-based hybrids onto the surface of core-shell MNPs was realized according to the strategy used in our previous works for the heterogeneization of POMs into mesoporous materials [8,10]. In this respect, this strategy consisted in the coupling of complementary functions, i.e. amine groups at the oxide-support (being mesoporous silica or MNPs in the present work) and carboxylic acid functions on the termination of the organic groups introduced in the POMs framework. The POM we used in both studies is the bis-phosphonyle derivative $TBA_3NaH(POM\text{-}CO_2H)$ ($(^{n}Bu_4N)_3NaH[As^{III}W_9O_{33}\{P(O)(CH_2CH_2CO_2H)\}_2]$) depicted in figure 1, which contains two independent carboxylic acid functions.

In the literature, silica-coated maghemite MNPs are prepared and generally used in aqueous media, regarding their applications in pharmaceutical and biomedical areas. However, in our case, we needed to stabilize these NPs in organic media, since the coupling reaction between amine and carboxylic acid functions was carried out in dried organic solvent, generally in acetonitrile or less commonly in DMF. Fortunately, we found that it was possible to prepare the core-shell NPs stabilized by PEG and aminopropyl chains in both solvents, after a simple redispersion in the corresponding solvent, assuming that their concentrations were adapted, leading typically to final concentrations in the range $5.5.10^{-7}$ (unsorted cores) - 10^{-6} $mol.L^{-1}$ (sorted cores).

Once stable suspensions of core-shell MNPs were obtained in acetonitrile, POMs were covalently immobilized at the surface of the MNPs. The formation of the amide bond was ensured using isobutylchloroformate, in the presence of triethylamine for the activation of the carboxylic acid functions found on POMs (see experimental section for details). It is noteworthy that we had to use a higher initial POMs:$\{NH_2\}$ (1:1) ratio compared to our previous studies for a more efficient grafting.

3.3 Characterization of POM-CO_2H-decorated core-shell MNPs.

The resulting colloidal suspensions were characterized by Dynamic Light Scattering (DLS), Diffuse Reflectance Infra-Red Fourier Transform Spectroscopy (DRIFT), X-ray photoelectron spectroscopy (XPS), Transmission Electronic Microscopy (including High Resolution techniques HR-TEM), magnetic measurements through superconducting quantum interference device (SQUID) and magnetic hyperthermia.

3.3.1 TEM studies

The samples of POMs-decorated MNPs were at first observed by classical transmission electronic microscopy to verify the shape, the aggregation and the integrity of the core-shell MNPs after the POMs grafting steps. The TEM micrographs in figure 2 showed that this grafting did not alter the intrinsic structure of the nanoparticles, despite the use of triethylamine and acetonitrile. The micrographs also hardly showed aggregation of the MNPs, most of them being isolated.

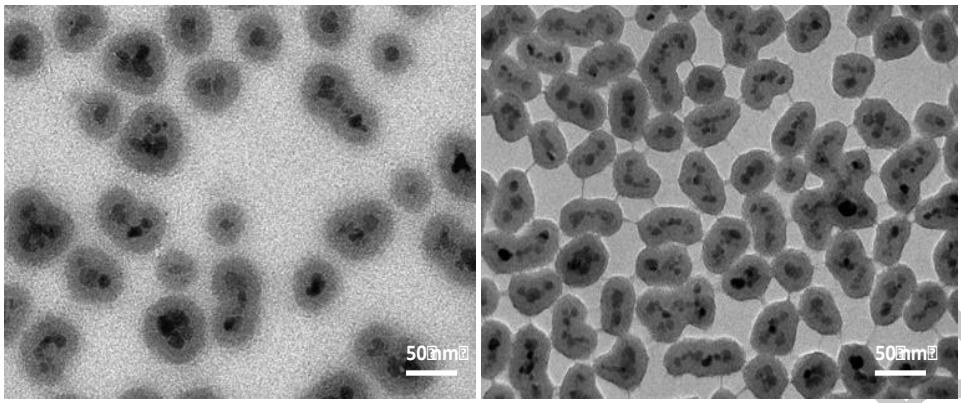

Fig. 2: TEM micrographs of a suspension of core-shell MNPs with unsorted cores (left) and POMs-decorated core-shell MNPs with unsorted cores (right) after 3 rinses.

In all samples, the nanoparticles have globally a round shape and the average number of maghemite cores by particle is about 3 (for sorted and unsorted cores). In the case of unsorted cores-containing MNPs, the average diameter was 47±8 nm (figure 3, left) based on the count of an assembly of 120 MNPs. The core-shell MNPs obtained with the sorted cores (9 nm) are barely larger, with an average diameter of 56±12 nm as shown on the size histogram on figure 3 (right), which results from the measurement of 228 particles.

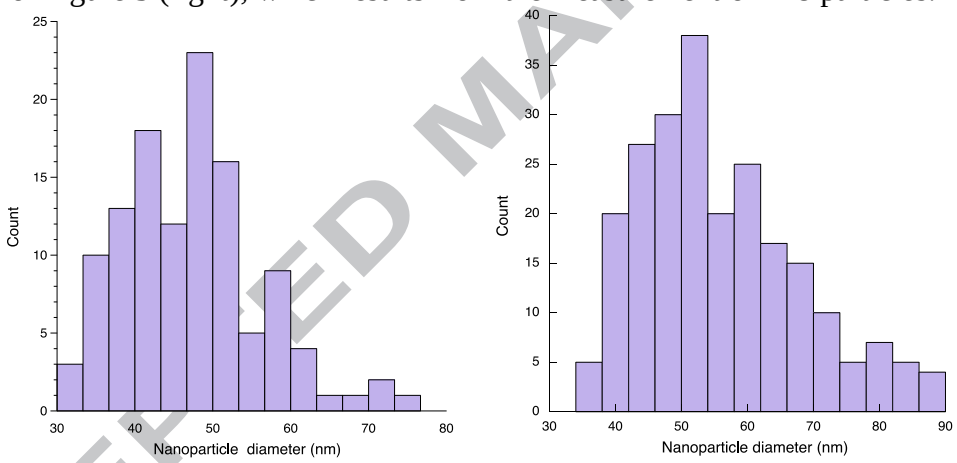

Fig. 3: Size histograms for POM-CO_2H-decorated MNPs sample with (**left**) unsorted and (**right**) sorted (9 nm) maghemite cores, counted from TEM micrographs.

Moreover some recent studies have proved that High-Resolution Transmission Electronic Microscopy can now be considered as a powerful tool for the precise characterization of POMs in nanomaterials [26]. We also used this technique in order to localize the POMs in the colloidal suspensions, in particular at different steps of their preparation. The samples micrographs obtained before the washing steps in figure 4a are instructive since it clearly shows individual POMs as isolated dark dots on the silica shells of MNPs. However, dark dots of POMs are also visible all around the particles at this step of the preparation. Examination of the elemental composition on different part of the samples by X-ray Energy-dispersive spectroscopy (XEDS, See Supplementary Material Fig. S1 to S4 for more details) confirmed that W atoms are present in each part of the samples, even far from the POMs-decorated MNPs.

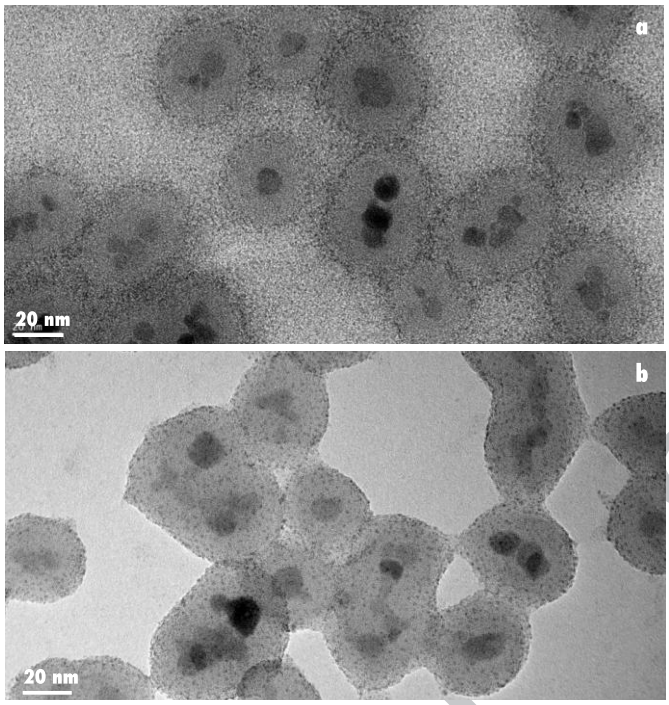

Fig. 4: HR-TEM micrographs of suspension of POMs-decorated core-shell MNPs with unsorted cores before (a) and after (b) washing and centrifugation steps.

On the contrary, the micrograph in figure 4b, recorded after rinsing, showed dark dots of POMs only at the surface of the MNPs. Furthermore, the presence of tungsten atoms (consequently of POMs) was not found by XEDS in between the MNPs (see Supplementary Material Fig. S3). The washing steps are thus sufficiently efficient to remove all non-grafted POMs from the suspension. In other words, with our covalent binding strategy the remaining, POMs are thus linked strongly enough to the organic shell of the MNPs to not be easily removed during the washing steps.

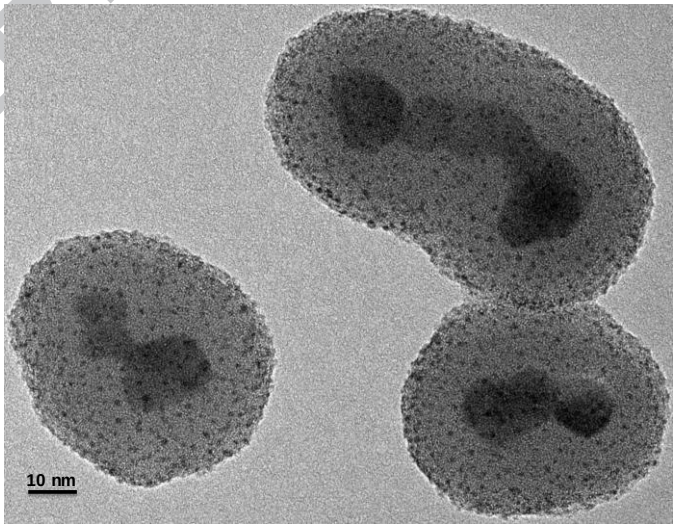

Fig. 5: HR-TEM micrograph of POMs-decorated MNPs with sorted cores showing POMs as black dots.

Figure 5 showed a magnification of a POM-CO_2H-decorated MNPs sample, with sorted (9 nm) maghemite cores. First, the presence of lattice fringes of the maghemite domains could be observed on the micrograph (see also Supplementary Material figure S6). This suggests that each core within the 2-3 core particles corresponds to a single nanocrystal. Furthermore, at this magnification the size of the black dots of POMs was measured and was

found at an average diameter of 1.0 nm, which corresponds to the size of isolated POMs and not to aggregates. It is also clear that the black dots of POMs are very regularly distributed at the surface of the whole MNP, leading apparently to an important coverage of the MNPs by POMs.

We thus tried to quantify precisely the POMs on the MNPs (with unsorted cores) by calculating the Si/Fe and Fe/W ratios by XEDS.

- For Si/Fe, we found the value equal to 7.9 by XEDS (average value on 16 different samples). This value is identical for both sorted and unsorted cores, but is lower than the initial theoretical ratio (11.1 for the unsorted cores and 9.5 for the sorted cores) between the different reagents introduced $(n_{TEOS} + n_{PEOS} + n_{APTES})/n_{Fe}$ during the synthesis of the MNPs. For sake of comparison, the Si/Fe ratio was found equal to 9.9 by ICP. This difference with XEDS results is certainly due to the fact that XEDS measurements are obtained on representative zones of the sample, but not on the whole sample. A possible explanation may be the presence of pure silica grains obtained during the synthesis, which were not taken into account during the HR-TEM observation.

- For Fe/W, we found an average value of 2.2 (± 0.5) by XEDS (average value on 16 different samples), compared to the 0.5 initial ratio of Fe from maghemite NPs over W of POM- CO_2H introduced. The average POMs grafting rate were thus estimated to 20%.

These results allowed us to propose a POMs composition for the POM-CO_2H-decorated MNPs.

For the MNPs with unsorted cores, knowing the iron concentration, the average diameter of maghemite cores (7 nm) and the average number of cores per MNP (3 cores), we were able to calculate the concentration of MNPs. The concentration of POMs, deduced form the Fe/W ratio determined by XEDS, divided by the concentration of MNPs showed that each POMs-decorated MNP is covered with an average of 1250 POMs per MNP. To give a rough idea of the compactness of the surface nanostructuration, we made an approximate calculation of the maximum number of POMs that might be arranged on the surface of a MNP. Then, assuming that the MNPs are spherical, with an average diameter equal to 47 nm, the available surface is about 7000 nm^2. In parallel, it is possible to evaluate the surface occupied by a POM by different methods. Using the X-ray diffraction data obtained with the crystal structure of $(^{n}\text{-}Bu_4N)_3NaH[As^{III}W_9O_{33}\{P(O)(CH_2CH_2CO_2H)\}_2]$ [17], we found approximately 1.8 nm^2. On the other hand, collision cross-section values obtained by Traveling Wave Ion Mobility-Mass Spectroscopy (TW-IM-MS) for tetrabutylammonium salts of POMs (including POM-based hybrids) are generally in the range of 2.0 – 2.5 nm^2 [27]. Regarding these different values, a compact coverage will lead to a maximum number of POMs in the range of 2800-3500 POMs *per* NP. In conclusion, the POMs coverage at the surface is pretty good (between 36 to 45 % of the total surface). This represents a grafting of approximately 19 % of the -NH_2 functions of the NPs, assuming that most of grafted POM entities are linked through only one amide function, as demonstrated previously on mesoporous SBA-15 supports [8].

In the case of POMs-decorated MNPs with sorted cores, the ratio Fe/W is higher, according to the larger size of the cores and was found equal to 5.1. However the number of grafted POMs (*ca.* 1000 POMs *per* NPs) determined by XEDS is in the same range despite a higher average surface (about 10000 nm^2). Consequently the POMs coverage (in the range 20-25%) is then slightly lower in this case. Approximately 16 % of the -NH_2 functions of the NPs are grafted, compared to 19% for the unsorted cores.

3.3.2 Dynamic Light Scattering Studies

Table 1 summarizes the average values of number-weighted hydrodynamic size of unsorted and sorted MNPs with or without POMs assayed by the DLS technique. The results presented below show that the average hydrodynamic diameter of all nanoparticles is in the

nanometer scale. As expected, the hydrodynamic diameter of nanoparticles is slightly increased in comparison with the nanoparticle diameter obtained at solid state measured by TEM. This is due to the solvation layer, not observed in TEM, and also probably to the existence of moderate aggregation phenomena occurring in an organic solvent like acetonitrile. However, all the measured hydrodynamic diameters are close to 100 nm and no micrometric aggregates were observed in those colloidal suspensions, even for sorted MNPs-POMs presenting the highest value of hydrodynamic diameter.

Nanoparticles	Hydrodynamic diameter (nm)	Polydispersity Index	Average size by TEM (nm)
Unsorted MNPs	90	0.177	47
Unsorted MNPs-POMs	90	0.081	
Sorted MNPs	80	0.107	56
Sorted MNPs-POMs	110	0.243	

Table 1: average number-weighted hydrodynamic diameter (DLS) and size measured by TEM.

Autocorrelation functions for all samples may be found as supplementary data, figure S14.

3.3.3 X-ray photoelectron spectroscopy (XPS) study

XPS spectrum was recorded on a solid sample of POMs-decorated MNPs, prepared by drying a suspension of these MNPs in acetonitrile (full survey spectrum displayed in Supplementary Material Fig S6). The high-resolution W4f, Si2p and N1s spectra are displayed respectively on figures 6, (Supplementary Material) S8 and 7.

The W4f peak was composed of a well-resolved spin-orbit doublet (35.4 and 37.6 eV for $W4f_{7/2}$ and $W4f_{5/2}$ respectively), typical of W^{VI} atoms in agreement with literature data on Keggin-type POMs [28,29]. In addition, the W4f peak displayed additional contributions observed at 34.1 and 36.3 eV that we attributed to a partial reduction of tungsten under X-ray irradiation [28]. The Si2p region of POMs-decorated MNPs (see Supplementary Material fig. S7) was characterized by a stronger contribution at 102.9 eV arising from the Si-C bonds of APTES functionalized surface. It is worth noting that the presence of Si^{IV} sites from the SiO_2 bulk (expected at *ca.* 104 eV) cannot be distinguished in the present spectrum.

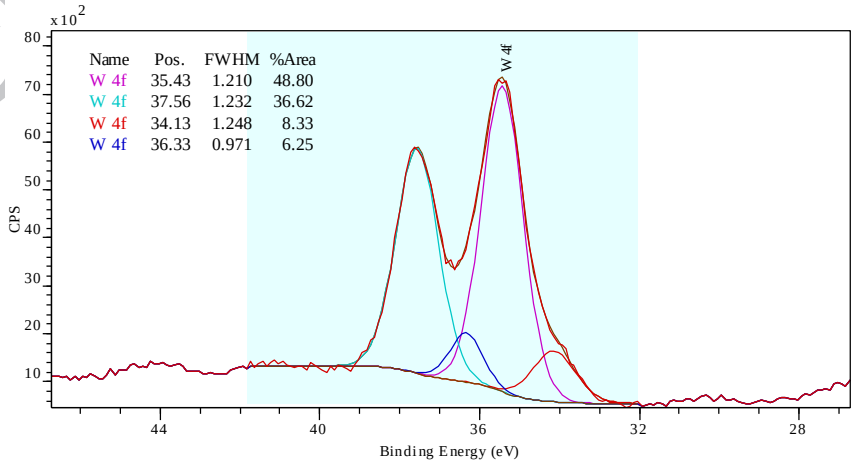

Fig. 6: High resolution W4f spectrum of dried POMs-decorated MNPs

The N1s region of the XPS spectrum (figure 7) was characterized by the presence of two peaks at 399.6 and 401.5 eV. The peak at 401.5 eV is characteristic of the presence of ammonium ions. In the present case tetrabutylammonium but also propylammonium (*i.e.*

protonated propylamine introduced with APTES) and triethylammonium ions are expected. The presence of the latter is due to the grafting step, *i.e.* to the deprotonation of the carboxylic functions of POM-CO_2H by triethylamine. The second peak at 399.6 eV may be associated to the propylamine functions covering the MNPs. We also intended to characterize the covalent link between the POMs and the MNPs, thus to identify the N atoms of the amide functions. However, these functions may be hardly distinguished from simple amine groups, since they are generally localized at energies under 400 eV.

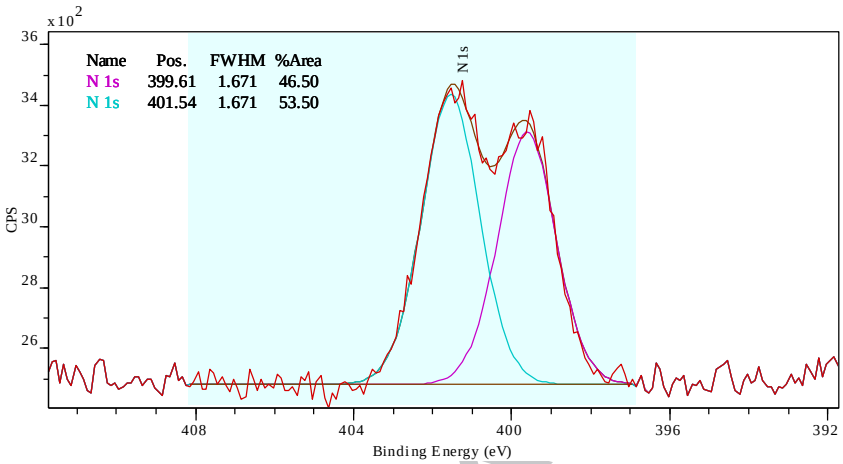

Fig. 7: High resolution N1s spectrum of dried POMs-decorated MNPs

Finally, we were not able to observe Fe peaks due to the high thickness of silica shells around the maghemite cores.

3.3.4 Diffuse Reflectance Infra-red Fourier Transform spectroscopy (DRIFT) study

DRIFT spectroscopy is the most efficient infrared technique for the characterization of molecules immobilized at the surface of a silica support (silica nanoparticles or bulk silica, including mesoporous materials) in particular in catalysis.[30] In DRIFT, the incident radiation underwent multiple reflections occurring at the surface of the particles and without penetrating the sample. However, DRIFT spectra may be extremely difficult to interpret because they closely depend on the conditions in which they are obtained. For this reason, all the infrared spectra presented in the present work were obtained with the same specific device (see experimental part) and recorded in DRIFT mode. No conversion of FTIR spectra (neither with an ATR device nor in classical transmission mode on KBr pellets) was done, since comparison between transmission and DRIFT modes are dangerous.

The DRIFT spectrum of POMs-decorated core-shell MNPs was recorded on solid samples obtained by drying a suspension of these NPs in acetonitrile. It was compared to that of TBA_3NaH(POM-CO_2H) and of dried core-shell NPs before the POMs functionalization (see figure 8). The spectra of the samples containing MNPs were mainly dominated by the bands of the maghemite cores at low energy (peaks at 695, 635 and 560 cm^{-1}) [31], and by those of the silica shell (805, 950 and 1090 cm^{-1}). However, the presence of the POMs may also be detected by a careful comparison of both spectra. Indeed, the intensity and the width of the bands at 805 and 950 cm^{-1} were found higher in the case of POMs-decorated core-shell MNPs. Having in mind the DRIFT spectrum of TBA_3NaH(POM-CO_2H) (figure 8, bottom), this is probably due to the superimposition with the most intense bands of the POMs (respectively at 780 and 965 cm^{-1}). More interestingly, a shoulder at 910 cm^{-1} was systematically observed in all the spectra of POMs-decorated MNPs, whatever the samples studied. This band was undoubtedly attributed to one of the $\nu(W{=}O_t)$ of the POMs, as it can be observed on the DRIFT spectrum of TBA_3NaH(POM-CO_2H).

Last but not least, the DRIFT spectrum of the POMs-decorated core-shell MNPs also displayed the complete disappearance of the band at 1727 cm^{-1} (ν(CO) of the carboxylic acid of POM-CO_2H) [32] and the presence of an additional weak feature at 1670 cm^{-1} (see also S10). This latter band can be easily distinguished from the δ(OH) at 1635 cm^{-1} of the residual water in the samples and was tentatively attributed to the ν(C=O) of an amide (amide I band). This would be a direct evidence of the covalent linking of the POMs at the surface of the MNPs. For sake of comparison, we also recorded the DRIFT spectrum of core-shell MNPs on which POMs were electrostatically deposited (see 2.3.6 for the experimental part and Supplementary Material figure S11 for the DRIFT spectra). In this case, no shoulder at 1670 cm^{-1} was observed, while a supplementary band at *ca.* 1720 cm^{-1}, close to the ν(CO) of the carboxylic acid functions of "free" POM-CO_2H anions.

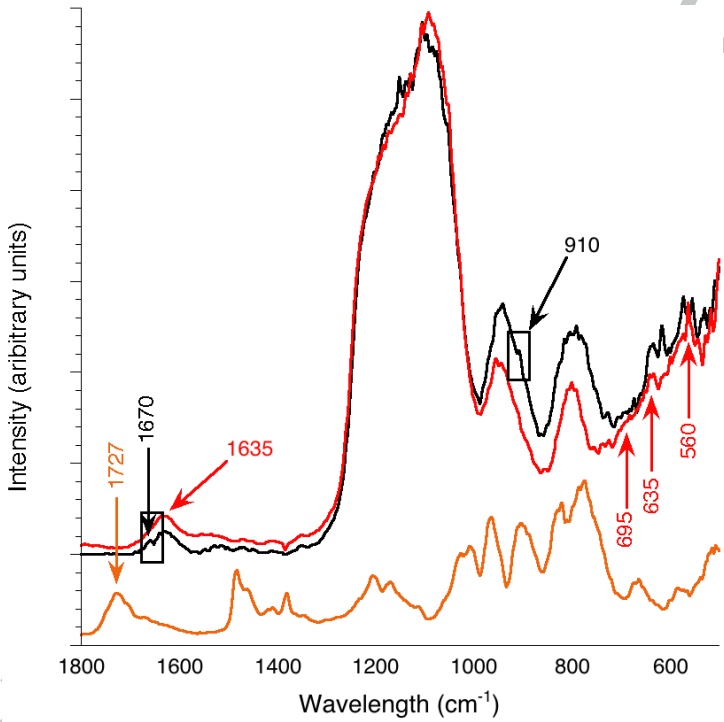

Fig. 8: Comparison of the DRIFT spectrum of POMs-decorated core-shell MNPs (in black) with those of core-shell MNPs (in red) and of TBA_3NaH(POM-CO_2H) (light brown)

3.3.5 Comparison between covalent linking strategy and electrostatic interactions

For sake of comparison, a "blank" sample obtained by a simple dispersion of the NH_2-functionalized MNPs in a solution of TBA_3NaH**(**POM-CO_2H) was prepared. We thus used the same ratio NH_2-functionalized MNPs/POMs-CO_2H as for the covalent grafting (see experimental parts **2.3.5** and **2.3.6**). Both samples were treated similarly: centrifugation (10000 rpm) during 20 minutes, repeated twice.

The resulting suspensions obtained after these centrifugations were also observed by HR-TEM in both cases (including XEDS measurements). In the samples obtained by simple electrostatic interactions, we observed on the micrographs (see Supplementary Material figure S12) a less homogeneous distribution of the POMs at the surface of the MNPs compared to the samples prepared by covalent grafting.

The W and Fe contents of the materials were also analysed by XEDS after each step (*i.e.* in the initial dispersion and after each centrifugation). For the sample obtained after covalent grafting, the Fe/W ratios obtained by XEDS were successively 0.5 (without washing)

then 1.15, and 1.71 after the different washing steps. This ratio was not significantly modified by additional washings/centrifugations, as expected for a covalent linkage.
For samples obtained by electrostatic interactions (either in DMF or CH_3CN) we also measured the Fe/W ratio at different steps. We thus found that the W content of these samples was dependent of the solvent. In DMF, which is more polar and dissociating than CH_3CN, the Fe/W ratio is significantly higher than in CH_3CN after 3 washing steps (5.17 in DMF *vs.* 1.83 in CH_3CN). In acetonitrile, the difference between the covalent and ionic samples is not as blatant as expected. However, we observed a slow decrease of the W contents after each additional washing step (Fe/W ratio > 2 after 5 washing cycles). One explanation for such a relatively high content of POMs in the case of electrostatically linked samples in acetonitrile could be due to the presence of PEG chains. Indeed, it has been recently shown that specific supramolecular interactions between PEG chains and POMs do exist. These are hydrophobic intermolecular forces between POMs and the $-CH_2$ groups of the PEG chains as demonstrated by ^1H NMR spectroscopy.[33] Furthermore these multipolar interactions can lead to the formation of POMs–PEG nanoassemblies when dispersed in water, the suspension of these nanoassemblies being stabilized by electrostatic repulsions between the negatively charged POMs.

All together, these results thus emphasize all the benefits of the POMs anchoring strategy at the surface of the MNPs, in terms of robustness (*i.e.* decrease of the lixiviation rate) of the materials and nanostructuration at once.

3.3.6 Magnetic measurements

Magnetic measurements were performed on acetonitrile suspension of core-shell MNPs with sorted ($5.5.10^{-7}$ $mol.L^{-1}$) and unsorted cores (10^{-6} $mol.L^{-1}$), covalently grafted or not with POMs at 25°C. The magnetization curves are presented in figure 9 and the measurements were reported as magnetization per gram of maghemite. Due to the larger mean diameter of the sorted γ-Fe_2O_3 nanoparticles compared to the unsorted ones, the saturation magnetization of the core-shell MNPs with sorted cores is higher (81 emu/g of maghemite) than the core-shell MNPs with unsorted cores (61 emu/g of maghemite). This difference in diameter of the maghemite nanoparticles also explains the larger magnetic susceptibility of the particles with the sorted cores compared to the unsorted ones, as the slopes at small field indicate (insert figure 9). As expected, the POM covalent grafting does not influence the magnetization properties of the core-shell MNPs with the unsorted cores, as the magnetic properties of the nanoparticles are solely due to the maghemite cores. However there is a slight difference between the saturation magnetization of the core-shell MNPs with the sorted cores before and after grafting of the POMs, due to measurement uncertainties during the estimation of the iron concentration in such diluted samples.

It is noteworthy that the weak divergence of both curves, observed during the temperature rise and fall steps, is generally attributed to the reorganization of magnetic nanoparticles under the magnetic field, leading to the formation of dipolar chains under the magnetic field [34].

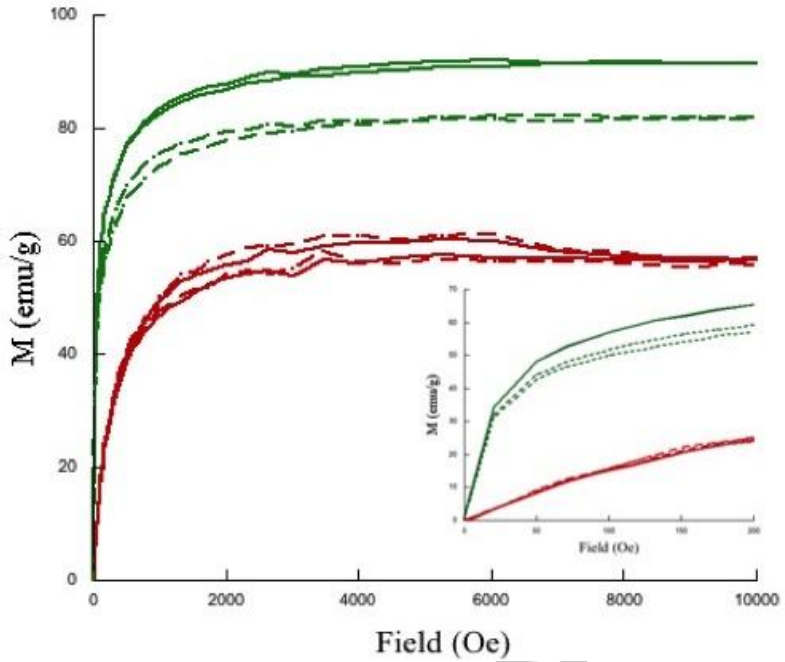

Fig. 9: Magnetization curves of acetonitrile suspension of core-shell MNPs with unsorted cores (red) (plain: non decorated, dash: POMs-decorated) and with sorted cores (green) (plain: non decorated, dash: POMs-decorated). The magnetization is given per gram of maghemite. Insert is a zoom in the range 0-200 Oe.

3.3.7 Magnetic hyperthermia properties

Magnetic hyperthermia properties were determined on core-shell MNPs with sorted and unsorted cores, covalently grafted or not with POMs. The temperature variation curves as a function of time for core-shell MNPs with sorted and unsorted cores, covalently grafted with POMs, are presented in figure 10.

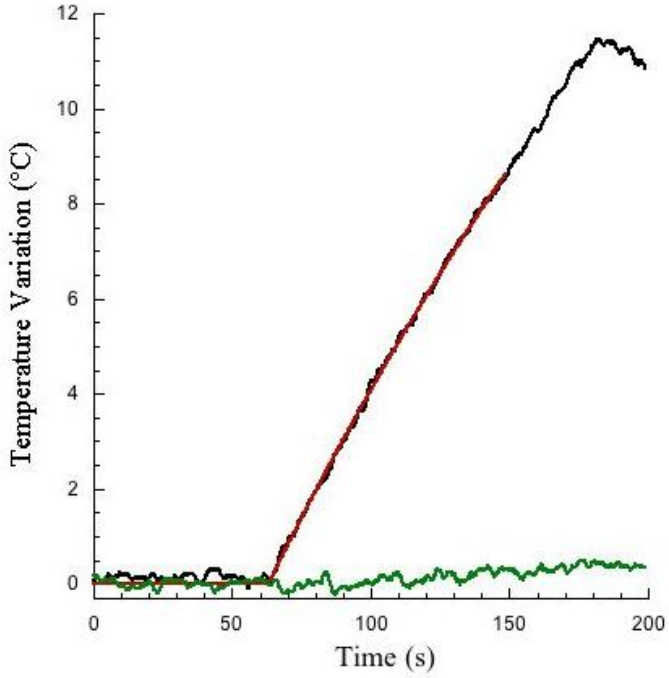

Fig. 10: Evolution of temperature variation over time under alternating magnetic field for POMs-decorated core-shell MNPs with sorted (black line) and unsorted cores (green line).

As expected for core-shell MNPs with smaller unsorted cores, no temperature variation was measured. On the contrary, an important increase of the temperature, around 1°C per ten seconds, was observed for core shell MNP with sorted cores once the alternating magnetic field was applied (t = 60 s).

The initial rise of the temperature, following the application of the field, was approximated by a linear increase as a function of time (red line in figure 10) and the slope dT/dt could thus be estimated. The specific loss power (SLP) was then calculated according to equation 1:

$$SLP = Cp\frac{m}{m_{MNP}}\frac{dT}{dt} \quad (1)$$

where Cp is the specific heat capacity of the solvent, m the mass of the sample and m_{MNP} the mass of magnetic nanoparticles in the sample. A value of Cp = 2.227 $J.g^{-1}.K^{-1}$ was used in acetonitrile.

The SLP calculated value of 52 $W.g^{-1}$ for POMs-decorated core shell MNPs with sorted cores is in good agreement with reported SLP values for such sorted magnetic nanoparticles[35]. Similar results were obtained while studying core-shell MNPs with sorted and unsorted cores, but not decorated with POMs (figure S13). An SLP of 66 $W.g^{-1}$ was calculated for core-shell MNPs with sorted cores. Comparison with the SLP of 52 $W.g^{-1}$ for the same nanoparticles with POM grafted onto their surfaces evidences that hyperthermic properties are in the same range after the surface decoration with catalysts.

4. Conclusions

In this manuscript, we presented the preparation of novel hybrid materials obtained by the covalent association of core-shell magnetic nanoparticles and polyoxometalate-based hybrids. For such a purpose, we used our well-established procedure for the coupling of the bis-propanoic acid phosphonyle POM derivative $(^{n-}Bu_4N)_3NaH[As^{III}W_9O_{33}\{P(O)(CH_2CH_2CO_2H)\}_2]$ (for short $TBA_3NaH(POM\text{-}CO_2H)$) with APTES-functionalized silica support. We thus succeeded in the preparation of POMs-decorated MNPs, in which the cores are constituted of crystalline maghemite domains. This strategy, as previously observed in the case of our POMs-functionalized mesoporous materials, allowed an excellent nanostructuration of the POMs shell at the surface of the core-shell MNPs, as determined by High-resolution Transmission Electronic Microscopy. We equally demonstrated that the covalent anchorage of POMs increased the link's strength between the POMs and the MNPs, especially during the separation and rinsing steps of the preparation of the materials. These two last results are of particular interest for the further use of these hybrid systems in supported catalytic processes, which is one important target of the study. As a result, the presence of the maghemite cores allows naturally their separation from colloidal solutions through the use of an external magnetic field. This characteristic potentially provides an easier way for POMs/catalysts recovery than using conventional catalysts supports.

Furthermore, these hybrid nanomaterials were stabilized in organic media (acetonitrile and dimethylformamide), thus facilitating their processing and their potential use as catalysts for the transformation of organic compounds. This is an important point of this study since most works referring to the use of such core-shell MNPs were performed in aqueous media.[36] The careful characterization of these materials was carried out using a full set of physical techniques including spectroscopic methods (DRIFT, XPS, X-EDS), High-resolution Transmission Electronic Microscopy, DLS and magnetic measurements. Additionally, we have shown that these hybrid materials displayed very good hyperthermic behaviour. We think that such hyperthermic behaviour is particularly relevant in the field of catalysis, by generating localized "hot points" at the surface of MNPs, at the exact place where the POMs are distributed. These materials may potentially be considered as the first hyperthermia-

assisted nanocatalysts described in the literature. Their catalytic activity will be then reported in due time.

Acknowledgements

This work was supported by the Centre National de la Recherche Scientifique (CNRS) and the Université Pierre et Marie Curie – Paris 6. The authors acknowledge support from the CNRS and the Ministère de la Recherche et de l'Enseignement Supérieur for a PhD fellowship to Miss Ourania Makrygenni, and from the European commission for the postdoctoral funding of Dr Emilie Secret on the FET-OPEN MAGNEURON project. Thanks to Drs Christophe Calers and Yanling Li for their help respectively with the XPS and SQUID measurements.

Notes

The authors declare no competing financial interest.

Appendix A. Supplementary material

Supplementary data associated with this article (Supplementary HR-TEM micrographs and XEDS spectra associated, XPS survey spectrum and high resolution Si2P XPS spectrum, IR spectrum of $TBA_3NaH(POM\text{-}CO_2H)$, DRIFT spectrum of POMs electrostatically deposited on core-shell MNPs, HR-TEM micrographs of core-shell MNPs electrostatically covered with $TBA_3NaH(POM\text{-}CO_2H)$, evolution of temperature variation over time under alternating magnetic field for core-shell MNPs with sorted and unsorted cores) and DLS autocorrelation functions for suspensions of MNPs can be found in the online version, at xxx.

[1] C. L. Hill, O. A. Kholdeeva, *In Liquid Phase Oxidation via Heterogeneous Catalysis: Organic Synthesis and Industrial Applications*, M. G. Clerici, O. A. Kholdeeva Eds. Wiley: New Jersey, 2013; 263-319; O. A. Kholdeeva, N. V. Maksimchuk, G. M. Maksimov, *Catal. Today*, 2010, **157**, 107-113. L.Cheng, K. Zhu, L.-H. Bi, A. Suchopar, M. Reicke, G. Mathys, H. Jaensch, U. Kortz, R.M. Richards, *Inorg. Chem.*, 2007, **46**, 8457-8459. M. Vazylyev, D. Sloboda-Rozner, A. Haimov, G. Maayan, R. Neumann, *Top. Catal.*, 2005, **34**, 93-99.

[2] W. Salomon, F.-J. Yazigi, C. Roch-Marchal, P. Mialane, P. Horcajada, C. Serre, M. Haouas, F. Taulelle, A. Dolbecq, *Dalton Trans.*, 2014, **43**, 12698-12705.

[3] N. V. Maksimchuk, M. N. Timofeeva, M. S. Melgunov, A. N. Shmakov, Y. A. Chesalov, D. N. Dybtsev, V. P. Fedin, O. A. Kholdeeva, *J. Catal.*, 2008, **257**, 315-323.

[4] S. Omwoma, W. Chen, R. Tsunashima, Y. F. Song, *Coord. Chem. Rev.*, 2014, **258-259**, 58-71.

[5] O. A. Kholdeeva, M. P. Vanina, M. N. Timofeeva, R. I. Maksimovskaya, T. A. Trubitsina, M. S. Melgunov, E. B. Burgina, J. Mrowiec-Bialon, A. B. Jarzebski, C. L. Hill, *J. Catal.*, 2004, **226**, 363-371; N. V. Maksimchuk, M. S. Melgunov, J. Mrowiec-Białon, A.B Jarzebski, O. A. Kholdeeva, *J. Catal.*, 2005, **235**, 175-183.

[6] R. C. Schroden, C. F. Blanford, B. J. Melde and B. J. S. Johnson, A. Stein, *Chem. Mater.*, 2001, **13**, 1074-1081.

[7] R. Zhang, C. Yang, *J. Mater. Chem.*, 2008, **18**, 2691-2703.

[8] R. Villanneau, A. Marzouk, Y. Wang. A. Ben Djamaa, G. Laugel, A. Proust, F. Launay, *Inorg. Chem.*, 2013, **52**, 2958-2965.

[9] A. Proust, B. Matt, R. Villanneau, G. Guillemot, P. Gouzerh, G. Izzet, *Chem. Soc. Rev.*, 2012, **41**, 7605-7622. G. Izzet, F. Volatron, A. Proust, *Chem. Rec.*, 2017, **17**, 250-266.

[10] F. Bentaleb, O. Makrygenni, D. Brouri, C. Coelho Diogo, A. Mehdi, A. Proust, F. Launay, R. Villanneau, *Inorg. Chem.*, 2015, **54**, 7607-7616.

[11] M. B. Gawande, A. Goswami, T. Asefa, H. Guo, A. V. Biradar, D.-L. Peng, R. Zboril, R. S. Varm, *Chem. Soc. Rev.*, 2015, **44**, 7540-7590.

[12] L. Harivardan Reddy, J. L. Arias, J. Nicolas, P. Couvreur, *Chem. Rev.*, 2012, **112**, 5818-5878.

[13] J. Kim, H. S. Kim, N. Lee, T. Kim, H. Kim, T. Yu, I. C. Song, W. K. Moon, T. Hyeon, *Angew. Chem. Int.l Ed.*, 2008, **47**, 8438-8441; P. H. C. Camargo, Z.-Y. Li, Y. Xia, *Soft Matter*, 2007, **3**, 1215-1222; R. Hao, R. Xing, Z. Xu, Y. Hou, S. Gao, S. Sun, *Adv. Mater.*, 2010, **22**, 2729-2742; R. Ghosh Chaudhuri, S. Paria, *Chem. Rev.*, 2012, **112**, 2373-2433; Y. Wang, H. Gu, *Adv. Mater.*, 2015, **27**, 576-585; Y. Lalatonne, C. Paris, J.-M. Serfaty, P. Weinmann, M. Lecouvey, L. Motte, *Chem. Commun.*, 2008, 2553; M. Niu, C.

Pham-Huy, H. He, *Microchimica Acta*, 2016, **183**, 2677-2695; Z. Sun, G. Cui, H. Li, Y. Liu, Y. Tian, S. Yan, *J. Mater. Chem. B*, 2016, **4**, 5194-5216.
[14] A. Ito, M. Shinkai, H. Honda, T. Kobayashi, *J. Biosci. BIoeng.*, 2005, **100,** 1-11.
[15] T. Georgelin, S. Bombard, J.-M. Siaugue, V. Cabuil, *Angew. Chem. Int. Ed.*, 2010, **49**, 8897-8901.
[16] F. Etoc, C. Vicario, D. Lisse, J.-M. Siaugue, J. Piehler, M. Coppey, M. Dahan, *Nano Lett.*, 2015, **15**, 3487-3494.
[17] R. Villanneau, D. Racimor, E. Messner-Henning, H. Rousselière, S. Picart, R. Thouvenot, A. Proust, *Inorg. Chem.* 2011, **50**, 1164-1166.
[18] R. Massart, J.-C. Bacri, R. Perzynski, D. Salin *J. Magn. Magn. Mater.* 1986, **62**, 36-46.
[19] M. Masteri-Farahania, J. Movassaghb, F. Taghavib, P. Eghbalib, F. Salimib, *Chem. Eng. J.*, 2012, **184**, 342-346. X. Zheng, L. Zhang, J. Li, S. Luo, J.-P. Chen, *Chem. Commun.*, 2011, **47**, 12325-12327.
[20] S. Wang, Z. Zhang, B. Liu, J. Li *Catal. Sci. Technol.*, 2013, **3**, 2104-2112.
[21] E. Rafiee, S. Eavani, *Green Chem.*, 2011, **13**, 2116-2122.
[22] Z. Zhang, F. Zhang, Q. Zhu, W. Zhao, B. Ma, Y. Ding, *J. Colloids Interface Sci.*, 2011, **360**, 189-194.
[23] M. Lévy, C. Wilhelm, J.-M. Siaugue, O. Horner, J.-C. Bacri, F. Gazeau, *J. Phys.: Condens. Matter*, 2008, **20**, 204133.
[24] C. Guibert, J. Fresnais, V. Peyre, V. Dupuis, *J. of Magn. Magn. Mat.*, 2017, **421**, 384-392.
[25] V. Maurice, T. Georgelin, J.-M. Siaugue, V. Cabuil, *J. Magn. Magn. Mater.*, 2009, **321**, 1408-1413.
[26] Y.Wang, I. A. Weinstock, *Chem. Soc. Rev.*, 2012, **41**, 7479-7496; Y. Wang, O. Zeiri, M. Raula, B. Le Ouay, F. Stellacci, I. A. Weinstock *Nature Nanotechnology*, 2016, **12**, 170-176; M. Zhang, J. Hao, A. Neyman, Y. Wang, I. A. Weinstock, *Inorg. Chem.*, 2017, **56,** 2400-2408.
[27] A. J. Surman, P. J. Robbins, J. Ujma, Q. Zheng, Perdita. E. Barran, L. Cronin, *J. Am. Chem. Soc.*, 2016**, 138**, 3824-3830.
[28] D. Mercier, S. Boujday, C. Annabi, R. Villanneau, C.-M. Pradier, A. Proust, *J. Phys. Chem. C*, 2012, **116**, 13217-13224.
[29] R. Villanneau, A. Roucoux, P. Beaunier, D. Brouri, A. Proust, *RSC Adv.*, 2014, **4**, 26491-26498.
[30] T. Armaroli, T. Bécue, S. Gautier *Oil & Gas Science and Technology – Rev. IFP*, 2004, **59**, 215-237.
[31] H. Namduri, S. Nasrazadani, *Corrosion Science*, 2008, **50**, 2493-2497.
[32] The absence of this particular band does not mean that all the $-CO_2H$ moieties reacted with the $\{NH_2\}$ functions of the core-shell MNPs. In particular, in the presence of triethylamine, these functions were deprotonated and consequently the ν(C=O) was then shifted in the range 1550-1610 cm^{-1}.
[33] T. Buchecker, X. Le Goff, B. Naskar, A. Pfitzner, O. Diat, P. Bauduin, *Chem. Eur. J.*, 2017, **23**, 8434-8442.
[34] K. Butter, P. H. H. Bomans, P. M. Frederik, G. J. Vroege, A. P. Philipse, *Nat. Mater.*, 2003, **2**, 88-91.
[35] J.-P. Fortin, C. Wilhelm, J. Servais, C. Menager, J.-C. Bacri, F. Gazeau, *J. Am. Chem. Soc.*, 2007, **129**, 2628-2635.
[36] J. Crassous, A. Mihut, H. Dietsch, O. Pravaz, L. Ackermann-Hirschi, A. M. Hirt, P. Schurtenberger, *Nanoscale*, 2014, **6**, 8726-8735.